universe

IMPACT FACTOR 2.9

CITESCORE 3.6

Article

A Study of Alpha-Particle Scattering on ^{10}B Nuclei at an Energy of 29 MeV

Maulen Nassurlla, Nassurlla Burtebayev, Stanislav Sakuta, Marzhan Nassurlla, Romazan Khojayev, Dilshod Alimov, Gulzada Baimbetova, Vyacheslav Dyachkov, Denis Zazulin, Avganbek Sabidolda et al.

MDPI

https://doi.org/10.3390/universe10010051

universe

MDPI

Article

A Study of Alpha-Particle Scattering on ^{10}B Nuclei at an Energy of 29 MeV

Maulen Nassurlla [1], Nassurlla Burtebayev [1,2], Stanislav Sakuta [3], Marzhan Nassurlla [1,*], Romazan Khojayev [1,2], Dilshod Alimov [1], Gulzada Baimbetova [4], Vyacheslav Dyachkov [2], Denis Zazulin [1,2], Avganbek Sabidolda [1,2], Yernazar Mukanov [1], Damir Issayev [1,2] and Akmaral Makhmut [2]

[1] Institute of Nuclear Physics, Ministry of Energy of Republic of Kazakhstan, Almaty 050032, Kazakhstan
[2] Department of Physics and Thechnology, Al-Farabi Kazakh National University, Almaty 050040, Kazakhstan
[3] NRC "Kurchatov Institute", Moscow 123182, Russia
[4] Depatment of Physics, Abai Kazakh National Pedagogical University, Almaty 050010, Kazakhstan
* Correspondence: nassurlla@yahoo.com

Abstract: The angular distributions of the elastic and inelastic scattering of α-particles on ^{10}B nuclei were measured at an energy of 29 MeV (with excitation of the 0.718 MeV (1^+) state). The data obtained by us, together with the angular distributions of the elastic scattering measured earlier in a wide range of energies from 24 to 90 MeV, were described using an optical model, the coupled-channel method, and parameterized phase analysis. The optimal parameters of optical potentials were found, and a good description of the experimental data in the specified energy range of α-particles was achieved. By taking into account the contribution of the elastic transfer mechanism of the ^{6}Li cluster, it was possible to correctly reproduce the rise of the cross section at the backward angles in the elastic channel. The value of the quadrupole deformation parameter was extracted from the analysis of inelastic scattering using the coupled-channel method. The geometric parameters of the interaction potentials were determined using parameterized phase analysis. The radii of the ^{10}B nuclei in the high-energy region (30 MeV and above) obtained by PPA are in good agreement with the radii calculated in the framework of the optical model.

Keywords: elastic scattering; optical potentials; coupled channels; phase analysis

check for updates

Citation: Nassurlla, M.; Burtebayev, N.; Sakuta, S.; Nassurlla, M.; Khojayev, R.; Alimov, D.; Baimbetova, G.; Dyachkov, V.; Zazulin, D.; Sabidolda, A.; et al. A Study of Alpha-Particle Scattering on ^{10}B Nuclei at an Energy of 29 MeV. *Universe* **2024**, *10*, 51. https://doi.org/10.3390/universe10010051

Academic Editor: Máté Csanád

Received: 7 November 2023
Revised: 8 January 2024
Accepted: 16 January 2024
Published: 22 January 2024

Copyright: © 2024 by the authors. Licensee MDPI, Basel, Switzerland. This article is an open access article distributed under the terms and conditions of the Creative Commons Attribution (CC BY) license (https://creativecommons.org/licenses/by/4.0/).

1. Introduction

Much attention has been and continues to be paid to the study of the scattering of α-particles by light nuclei. The reason for this interest is that the interaction of α-particles with light nuclei is ambiguous. The angular distributions (ADs) of α-particles scattered on light nuclei at large angles behave completely differently than on heavier nuclei. In the first case, the ADs, at least in the region of the front hemisphere, usually have a clearly defined diffraction structure that is well described by various diffraction and optical models. However, at large angles at low and medium energies, the elastic scattering cross sections (CSs) often show an increase that cannot be reproduced within the standard optical model. For heavier nuclei, the situation is different. Thus, an optical model analysis of the elastic scattering of α-particles at an energy of about 25 MeV on a large number of nuclei from oxygen to uranium [1] showed that for medium and heavy nuclei, there is a good description of experimental cross sections in the entire angular range; but for light nuclei (in regions of oxygen and silicon), especially at large angles, there is much less agreement between the experiments. A similar result was also obtained in [2] when analyzing elastic scattering on nuclei up to lead at energies of 22 and 40 MeV. During the past decades, using the optical model [3], a large amount of work has been conducted to determine the optical potentials in the interaction of alpha-particles with nuclei. By studying the elastic scattering of alpha-particles on ^{40}Ca and ^{90}Zr nuclei at an energy of 141.7 MeV, as well as on other nuclei at the same energy [4], it was shown that refractive effects are clearly

manifested in the region of intermediate energies. All the elastic scattering differential cross sections exhibited an exponential-like fall-off at large angles characteristic of nuclear rainbow scattering. For each nuclide studied, a unique family of Woods–Saxon optical potentials were obtained by fitting calculated cross sections to the experimental data, which made possible the elimination of the discrete ambiguity in the real part of the potential. The real parts of the extracted potentials are characterized by well depths ranging from 108 to 118 MeV and volume integrals $J/4A$ ranging from 297 to 352 MeV fm^3. In [5], the refractive, elastic scattering data on ^{12}C, ^{16}O, ^{58}Ni, and ^{90}Zr targets were analyzed within the optical model using double folding potentials. The folding parameters obtained for targets in different mass regions provide a useful guide in predicting the properties of optical potentials in the interaction of alpha-particles with nuclei in the study of elastic scattering (see also [6]). In [7], an analysis was carried out of all available cross sections for reactions caused by alpha-particles on nuclei in the mass number range $121 < A < 197$ at energies below the Coulomb barrier. This analysis revealed an optical potential that describes the α-particle elastic scattering at low energies. It was shown that the presence in the potential of the imaginary part of the term describing surface absorption, along with the term describing volume absorption, is very significant. Despite progress in determining optical potentials within the optical model, the problem of anomalous large-angle scattering for light nuclei still remains very relevant.

There are many mechanisms to explain this phenomenon (for example, the glory effect [8–10] and Regge poles [11–16]), which leads to uncertainty in the interpretation of experimental data. The scattering cross sections can also be influenced by the cluster structure of light nuclei, which can lead to the contribution of exchange processes with the transfer of clusters [17–22], as well as higher-order processes described by triangular and rectangular diagrams of the dispersion theory [23,24]. In addition to the processes listed above, one must also keep in mind the possible contribution of the mechanism of compound nucleus formation. At present, a large amount of information has been obtained on the inelastic scattering of various nuclear particles on 1p-shell nuclei, including the scattering of α-particles. It should be noted that the ^{10}B nucleus in the middle of the p-shell is strongly deformed, which is reflected in the large value of the nuclear quadrupole moment (Q = +84.72 mb) [25,26]. Therefore, in the analysis, it is necessary to take into account the collective nature of the 0.718 MeV (1^+) state of the ^{10}B nucleus. This is supported by the results of two studies that investigated the reactions, ^{11}B(α, t)^{12}C [27] and ^{11}B(d, t)^{10}B [28], which show the importance of taking into account the deformation of the ^{11}B and ^{10}B nuclei. In these works, the spectroscopic factors and parameters of quadrupole deformation of the nuclei under study were extracted from the analysis of experimental data within the coupled-channel method. This work is devoted to the study of elastic and inelastic scattering of α-particles on ^{10}B nuclei at the energy of 29 MeV. Angular distributions of elastic scattering were previously studied in the energy range E_α = 5–50 MeV [29,30] and 91.8 MeV [31], where a well-defined diffraction structure in the front hemisphere was observed together with the significant increase in the cross sections at the larger angles. In [29], the elastic scattering ^{10}B + α was measured at energies from 5 MeV to 30 MeV. Experimental data were analyzed using an optical model, the strong absorption model, and the Regge pole diffraction model. It was difficult to reproduce the angular distributions over the whole angular range from 20° to 170° with these models. Only the parts with a good diffraction pattern could be fitted well. In [30], the increase in cross sections at large angles was associated with spin–orbit interaction. It was found that the calculated curves using the optical model describe the experiment well only up to angles around θ = 120°. The reason for the poor description may be that the analysis of elastic scattering in [29–31] did not take into account the effects of channel coupling [32] and the exchange mechanism transfer of the ^{6}Li nucleus associated with the cluster structure of the ^{10}B nucleus (^{10}B$\rightarrow^6$Li+α).

The purpose of this work is to provide a more detailed description of the scattering of α-particles on ^{10}B nuclei, taking into account the coupling of channels and cluster exchange

effects, as well as a discussion of the problem of choosing the optimal potentials and determining the geometric parameters of the interaction potentials based on parameterized phase analysis.

2. Experimental Setup

An experiment to study the scattering of α-particles on ^{10}B nuclei was carried out on a beam of a U-150M isochronous cyclotron of the Institute of Nuclear Physics (Almaty, Republic of Kazakhstan) at E_α = 29 MeV. The beam intensity was controlled by means of a Faraday cup. The error of the current measurement did not exceed 1%.

The target was a self-sustaining 0.2 mg/cm^2 thick boron film with ^{10}B enrichment up to 90%. The film was made by the evaporation of boron samples using a point beam of accelerated electron ions in a special vacuum chamber. Its thickness was determined by the energy loss of α-particles from a radioactive source with an accuracy of about 7%. Charged particles, products of nuclear reactions were recorded by a telescope consisting of two silicon detectors: a thin one (ΔE) with a thickness of 30 to 50 microns and a thick one (E) with a thickness of 1–2 mm, depending on the maximum energy of the scattered particles. When measuring energy spectra in the reverse hemisphere, sets of detectors with smaller thicknesses were used. The identification of the type of charged particles was carried out using a two-dimensional analysis system (ΔE-E) with standard CAMAC and ORTEC electronics and a processing program implemented on a personal computer. A typical energy spectrum of α-particles scattered on ^{10}B nuclei at an angle of 55^0 is shown in Figure 1. The energy spread of the beam was about 300 keV. Peaks have been identified in the spectrum of scattered α-particles for the ground state of the ^{10}B nucleus ($J^\pi = 3^+$) and for its excited states, 0.718 MeV ($J^\pi = 1^+$), 2.154 MeV ($J^\pi = 1^+$), and 3.587 MeV ($J^\pi = 2^+$), as well as a peak in channel 118, as a possible sum of two undivided levels of 5.919 MeV ($J^\pi = 2^+$) +6.025 MeV ($J^\pi = 4^+$) of the ^{10}B nucleus. At these angles, the peak from the ground state of the ^{11}B nucleus ($J^\pi = 3/2^-$) is well separated from the elastic peak ^{10}B. The peaks for the ground state ($J^\pi = 0^+$) and for the first excited state 4.44 MeV ($J^\pi = 2^+$)) of the nucleus ^{12}C, as well as the peak from the ground state of the nucleus ^{16}O ($J^\pi = 0^+$), are clearly visible. These impurities could appear during the manufacture of the target and during its use in experiments due to the presence of residual gases and oil vapors in vacuum systems. The angular distributions of the differential cross sections of the scattering of alpha-particles on ^{10}B nuclei were measured in the range of angles θ_{lab} = 20–160° in increments of 2 degrees.

The angular uncertainty of the detector telescope installation was no more than 0.3 degrees. The systematic error in the cross sections is associated with the uncertainty of the target thickness, the angle of installation of the detectors, and the calibration of the current integrator, and it did not exceed 10% in total. The statistical error of the measured data was in the range of 1–5% and only in some cases reached 6–15% in the section minima at large angles (for inelastic scattering).

Figure 2 shows the measured angular distributions of the elastic and inelastic scattering with excitation of the ^{10}B state with an energy of 0.718 MeV (1$^+$). As can be seen from the figure, a well-defined diffraction structure is observed in the region of the angles of the front hemisphere, while the diffraction extreme for elastic and inelastic scattering is in the antiphase. At large angles, a significant increase in the elastic scattering cross sections and a damping of the diffraction structure are observed.

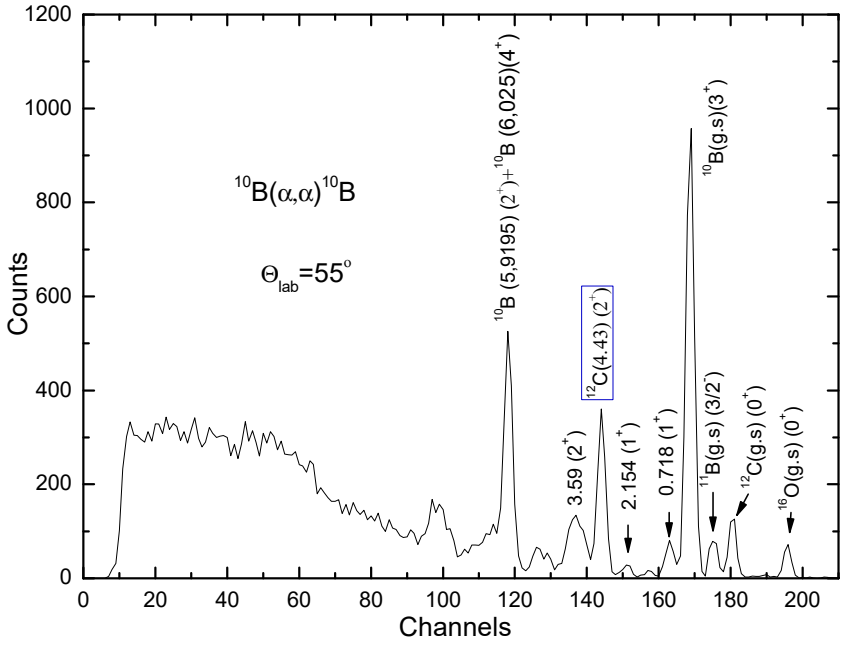

Figure 1. Measured at an angle of 55°, the energy spectrum of α-particles scattered on ^{10}B nuclei at a beam energy of 29 MeV.

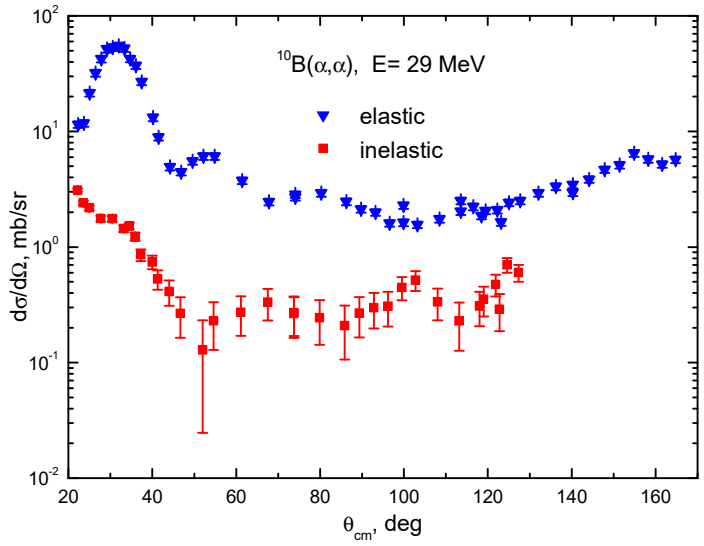

Figure 2. Angular distributions of differential cross sections for scattering of α-particles on ^{10}B nuclei at an energy of 29 MeV. Blue dots represent elastic scattering, and red dots represent inelastic scattering with excitation of the nuclear state ^{10}B 0.718 MeV (1$^+$).

3. Analysis and Discussion of the Results

3.1. Elastic Scattering and Optical Potentials

In the first stage, analysis of scattering was carried out according to the optical model (OM) using the SPI-GENOA program [33,34]. To date, a series of studies have been carried out to examine the elastic scattering of alpha-particles on different nuclei in the energy range from 20 MeV to 40 MeV [1,2,35,36]. Analysis of the experimental data on an optical model based on Woods–Saxon potentials showed that these potentials describe the measured angular distributions quite well. However, the depths of the real part of the potentials extracted from fitting the calculated cross sections to the experimental values vary from ~40 MeV to ~200 MeV, and the depths of the imaginary part vary from ~10 MeV to ~25 MeV.

In this work, the optimal parameters of the phenomenological optical potential (OP) were also found by comparing the calculated cross sections with the experimental data. Typically, a potential with the Woods–Saxon parameterization is used, the form of which with the volume absorption can be represented as

$$U(r) = -V_0\left(1 + exp\frac{r - R_v}{a_v}\right)^{-1} - iW_0\left(1 + exp\frac{r - R_w}{a_w}\right)^{-1} + V_C(r), \quad (1)$$

where V_0 and W_0 are the depths of the real and imaginary parts of the potential, respectively, $R_i = r_i A_t^{1/3}$ is the radii of the real (v) and imaginary (w) parts of the potential, and a_V and a_W are the corresponding diffuseness. The radius of the Coulomb potential V_C was assumed to be $R_C = 1.28 A_t^{1/3}$.

The optimal parameters of the optical potentials, corresponding to the best description of the experimental cross sections, were found by minimizing the value of χ^2:

$$\chi^2 = \frac{1}{N}\sum_{i=1}^{N}\left[\frac{(\sigma_i)_T - (\sigma_i)_E}{(\Delta\sigma_i)_E}\right]^2, \quad (2)$$

where N is the number of experimental points in the angular distribution, σ^T and σ^E are the calculated and measured values of the differential scattering cross section at an angle θ_i, and $\Delta\sigma^E$ is the uncertainty in the value of σ^E.

It should be noted that when choosing this potential as optimal, we were guided by the physically justified value of the volume integral of the real part of the OP, defined as

$$J_V = -(4\pi/A_p A_t)\int V(r) r^2 dr, \quad (3)$$

where A_p and A_t are the mass numbers of the incident particle and the target nucleus. The value of J_V should correspond to the value of the nucleon–nucleon interaction potential and should be equal to ~400 MeV·fm^3.

It is well known that OP parameters have discrete and continuous ambiguities. To eliminate the discrete ambiguity of the real part of the potential, its dependence on energy is often used.

For this purpose, a global systematization of the OP parameters was carried out to describe the scattering of α-particles at ^{10}B in a wide energy range. The calculations used experimental data obtained previously at energies of 91.8 MeV [31], 50.6 MeV [30], 30 MeV [29], 24 MeV [29], and 29 MeV (this work). In addition, our data on elastic scattering at E = 50.5 MeV, measured in the full angular range, were used in the analysis [37].

Subsequently, the search for optical potential parameters was carried out by selecting the OP parameters in such a way as to achieve the best agreement between the theoretical and experimental angular distributions using the FRESCO computer code [38]. To obtain physically based OP parameters, the recommendations given in [39] for α-particle scattering were used. The values of the reduced radii of the interaction potential obtained in this work from the global dependence of the OP parameters r_v = 1.245 fm and r_w = 1.57 fm were fixed, and fitting the theory to the experiment was carried out by varying the remaining four parameters of the OP (V_0, W_0, a_V, and a_W). The obtained optical potentials are listed in Table 1.

To avoid the influence of other mechanisms on the OP parameters, in addition to purely potential scattering, the fit to the experimental data was carried out in the region of the angles of the front hemisphere (OP set A). Additionally, to assess the influence of continuous ambiguity, another parameter was adjusted: the depth of the imaginary part of the potential W_0 (set B). In this case, a slight change in the quality of the fit is observed in the region of medium and large angles at low energies with a more pronounced diffraction structure due to the existence of a correlation between the depth and diffusivity of the imaginary potential (see Figure 3).

Table 1. Optimal parameters of optical potentials for the ^{10}B + α system.

E, MeV	Set	V_o, MeV	a_V, fm	W_o, MeV	a_w, fm	J_V	J_W	χ^2/N
24	A	155.04	0.742	18.29	0.666	545.05	102.46	97.82
	B	152.86	0.835	11.7	0.588	599.24	58.23	65.55
29	A	152.9	0.730	16.2	0.749	530.07	97.39	45.73
	B	140.9	0.730	23.63	0.740	488.25	140.96	68.46
	C	79.84	0.803	13.49	0.824	301.44	86.66	39.04
	D	215.4	0.545	12.20	1.07	606.58	98.23	28.87
30	A	147.23	0.756	13.41	0.869	531.67	109.2	48.96
	B	143.2	0.756	13.62	0.840	512.27	88.79	42.84
50.6	A	111.2	0.810	17.57	0.820	423.3	112.47	49.67
	B	119.77	0.726	15.47	0.93	413.29	109.43	31.17
91.8	A	105.56	0.831	20.24	1.01	412.04	154.29	6.392
	B	104.89	0.8	15.0	0.9	394.62	147.59	11.1

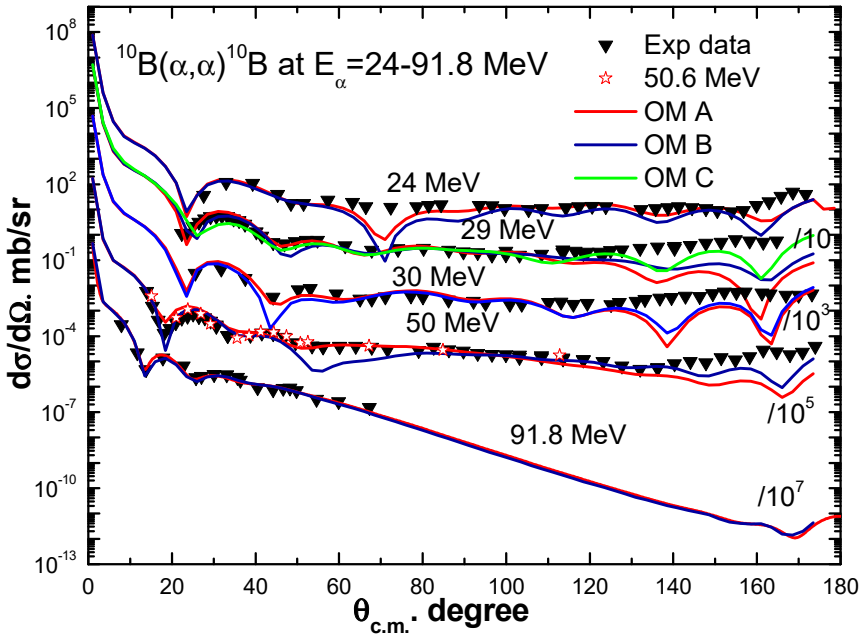

Figure 3. Angular distributions of differential cross sections of α-particles scattered on ^{10}B nuclei at energies of 24, 29, 30, 50, 91.8 MeV (red curve calculated with set A, blue curve with set B, and green curve with set C). Experimental data were taken from the following works: 24 and 30 MeV [29], 50.6 MeV [31], 50.5 [37].

A comparison of the calculated and experimental angular distributions of the elastic scattering of α-particles on ^{10}B nuclei at energies of 24, 29, 30, 50.5, 50.6, and 91.8 MeV is shown in Figure 3 for two potentials, A and B. As can be seen from the figure, the OPs from Table 1 describe the literature and our experimental data quite well, which indicates the correctness of the obtained OPs. The exception is the sharp increase in the experimental cross sections at large angles at low energies. To describe this increase in cross sections at large angles, it is most likely necessary to take into account the contribution of the elastic cluster exchange mechanism for the α+^{10}B system.

Potentials calculated within the framework of the double folding model (DFM) were used to test the OP parameters. In the DFM framework, the real part of the optical potential

is obtained by folding the effective nucleon–nucleon interaction with the nuclear densities of the projectile and target. The DFM coordinate system is presented in Figure 4.

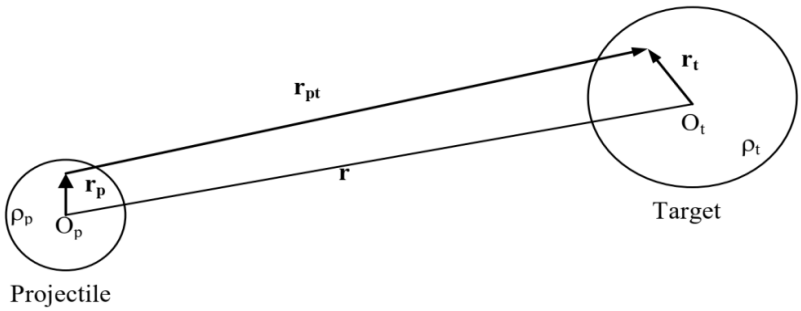

Figure 4. Coordinate system for DFM.

The DFM potential is determined by the expression

$$V^{DF}(r) = \int \rho_p(r_p)\rho_t(r_t)v_{NN}(r_{pt})d^3r_p d^3r_t, \tag{4}$$

where $r_{pt} = |r + r_t - r_p|$ is the distance between nucleons in the (fm), $\rho_p(r_p)$, and $\rho_t(r_t)$ density distributions of the projectile and target. Thus, the total optical potential $U(r)$ is written as

$$U(r) = -N_r V^{DF}(r) - iW(r) + V_C(r), \tag{5}$$

where $V^{DF}(r)$ is the DFM potential, and N_r is the renormalization coefficient of the real part of the optical potential, which can be adjusted to reproduce the elastic scattering data.

To calculate DFM potentials, several types of nucleon–nucleon V_{NN} interaction potential can be used. Among these different types of effective interactions, the so-called M3Y (Michigan 3 Yukawa) interaction has been widely used to calculate the optical potential of heavy ions [6,40,41]. In this work, DFM potentials were calculated using the DFPOT program [42] within the framework of a realistic nucleon–nucleon M3Y interaction, which is determined by the expression

$$v_{NN}(r) = 7999\frac{\exp(-4r)}{4r} - 2134\frac{\exp(-2.5r)}{2.5r} + J_{00}(E)\delta(r)MeV, \tag{6}$$

where $J_{00}(E)$ is the exchange part, parameterized as [43]

$$J_{00}(E) = -276\left[1 - 0.005\frac{E_{Lab}}{A_p}\right]MeVfm^3 \tag{7}$$

In the DFM calculations, the density distributions of projectile nuclei (^{4}He) and targets (^{10}B) were used in the Gaussian form as follows:

$$\rho(r) = \rho_0 \exp\left(-\beta r^2\right), \tag{8}$$

where ρ_0 can be determined using the normalization condition

$$\int \rho(r)r^2 dr = \frac{A}{4\pi}\ , \tag{9}$$

To calculate the densities, $< r^2 >^{1/2}$ radii for the ^{4}He target were chosen—1.68 fm and ^{10}B—2.45 fm [44]. The real part of the interaction potential calculated within the framework of the DFM was used to describe the data at an energy of 29 MeV with the imaginary part of the potential from set A. In this case, the normalization coefficient N_r was equal to one.

The results of the description of the angular distributions of elastic scattering are shown in Figure 5 in purple.

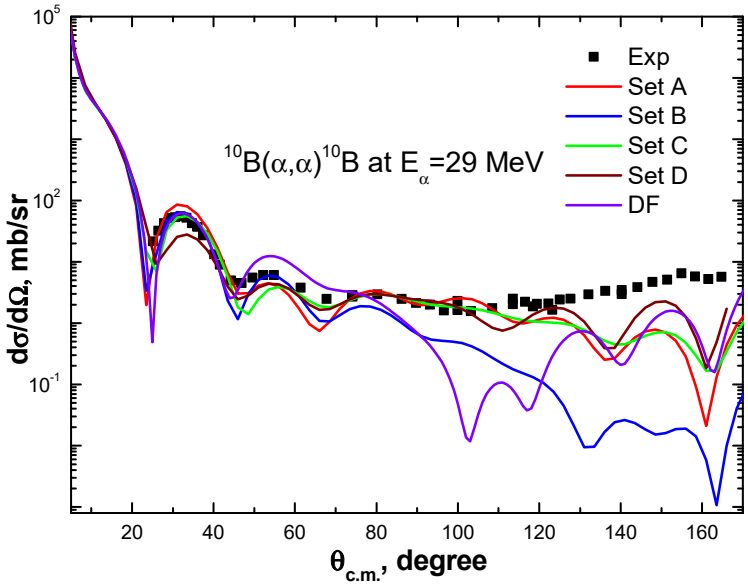

Figure 5. Angular distribution of differential cross sections of α-particles elastically scattered on ^{10}B nuclei at energy of 29 (red curve calculated with set A, blue curve—with set B, green curve—with set C, wine curve—with set D, and purple curve—with potential DF (N_r = 1)).

For an energy of 29 MeV, several more sets of OP parameters (C and D) were found. In this case, all potentials reproduce experimental data on elastic scattering equally well. As expected, the deep real potential (set D) produces a significant increase in cross sections at large angles, but it is still insufficient to reproduce the experimental cross sections (see Figure 5).

To study the dynamics of the discrete ambiguity when determining the depth of the real part of the potential, the radii and diffuseness of the real and imaginary parts of the potentials, as well as the depth of the imaginary potential A, were fixed for all energies. Using these parameters, the values of χ^2 were found for the real part of the optical potential in the depth range from 50 MeV to 240 MeV with a step of 10 MeV. Thus established, the dependence of χ^2 on the depth of the real part of the potential for each amount of energy of the incident particles is shown in Figure 6.

It can be seen that at low energies, several minimums are observed for χ^2. As the energy of the incident particles increases, the number of minimums decreases, which makes it possible to reduce the discrete ambiguity and reduce the number of optical potentials to one optimal when increasing the energy of colliding particles up to 91 MeV.

Figure 7 shows the radial dependences of the real (V) and imaginary (W) potentials for all used sets of OPs at E = 29 MeV.

As can be seen from the figure, the values of V and W for different sets of optical potentials intersect at different distances in the range from ~4 to ~8 fm. Such a wide range of potential crossings is most likely associated with the increasing role of continuous ambiguity in the parameters of the optical potential at low energies. At the same time, the values of the microscopic potential DF are close to the values of the potentials (sets A and B) in the region of the strong absorption radius (r~4 fm).

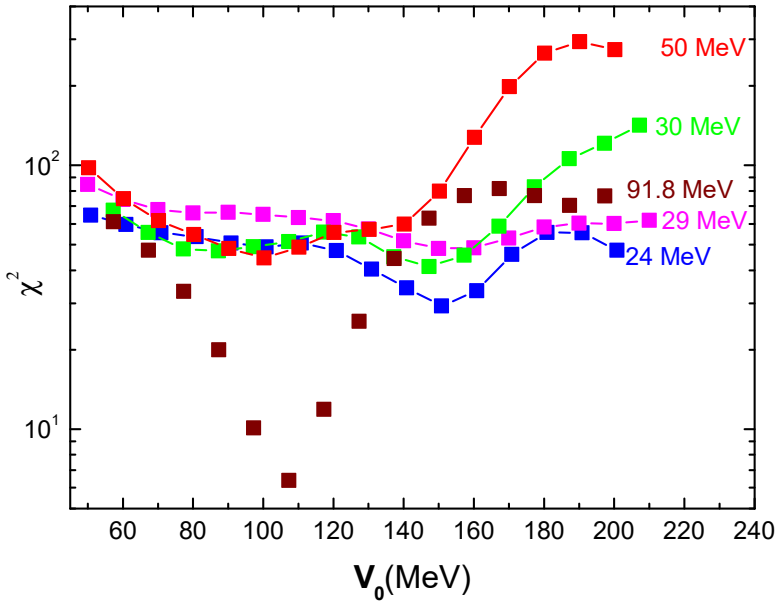

Figure 6. Dependence of χ^2 on V_0—the depth of the real part of the potential for α-particles.

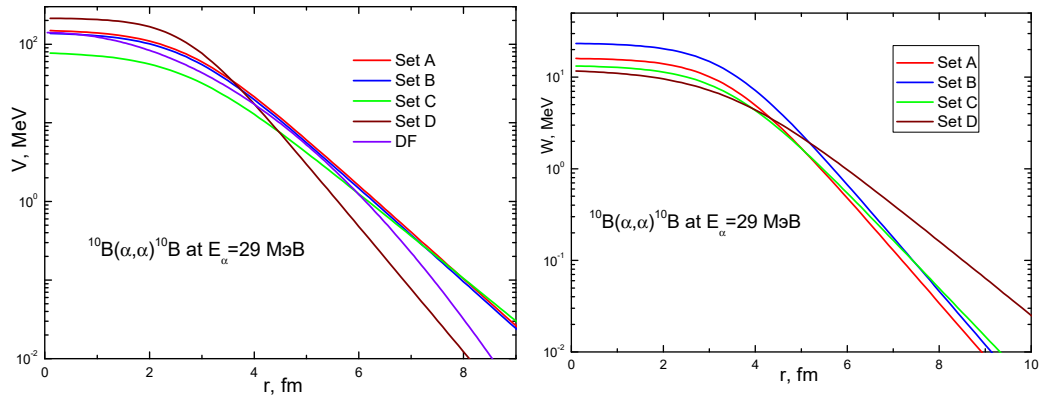

Figure 7. (**a**) Radial dependence of V. (**b**) Radial dependence of W.

3.2. Parameterized Phase Analysis of Elastic Scattering

To determine the geometric parameters of the interaction potential of ^{10}B and alpha-particles in their elastic scattering, we used parameterized phase analysis (PPA). In this approach, to describe experimental differential cross sections, the scattering amplitude is expanded into a series of partial waves and written in the form [45–48]

$$\mathrm{A}(\theta) = \frac{1}{2\mathrm{ik}} \cdot \sum_{l=0}^{\infty} (2\mathrm{l}+1) \cdot B_l \cdot \mathrm{e}^{2\mathrm{i}\sigma_l} \cdot \mathrm{P}_l(\cos(\theta)), \tag{10}$$

where the elements of the scattering matrix $\mathrm{B}_l = \frac{1}{1+\mathrm{e}^{\frac{\mathrm{l}_1-\mathrm{l}}{\lambda_1}}} + \mathrm{i}\frac{\mathrm{b}}{\mathrm{ch}^2\left(\frac{\mathrm{l}-\mathrm{l}_2}{\lambda_2}\right)}$.

Here, l_1, λ_1, l_2, λ_2, and b are the free parameters of the theory. They have the form shown in Figure 8.

The scattering matrix contains a real part, which is responsible for refraction, and an imaginary part, which is responsible for absorption.

In the analysis of elastic scattering, experimental data obtained previously at energies from 5 MeV to 91.8 MeV were used [29–31].

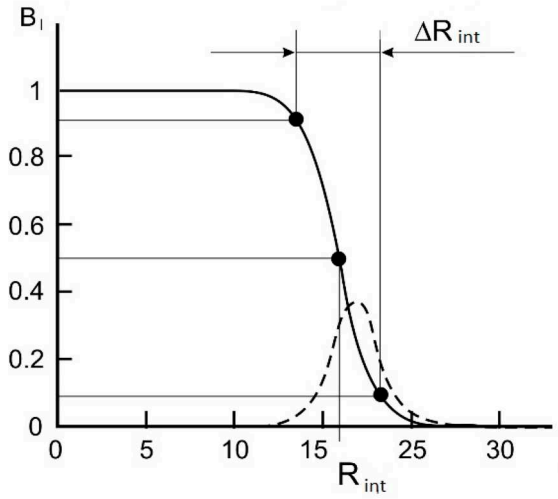

Figure 8. Elements of the matrix B_l depend on the angular momentum l of the incident particles. Solid curve—Re(B_l); dotted curve—Im(B_l). For Re(B_l), the values of R_{int} and ΔR_{int} are shown in the figure. For Im(B_l), the corresponding geometric absorption parameters are determined by the maximum and width at half maximum.

Using the angular distribution, we measured at an energy of 29 MeV, and with the angular distributions measured in [29–31], the parameters of the scattering matrix were determined by fitting with unambiguous minimum values of χ^2/N for five free parameters of the theory [49]. The number of partial waves over which summation occurs in (4) was selected for each amount of energy to obtain its optimal value, which varied around 25.

For optimal free parameters, the interaction radius was calculated:

$$R_{Int} = \frac{1}{k}\left(\eta + \sqrt{\eta^2 + l_1(l_1+1)}\right),$$

where k is the wave number, and $\eta = \frac{Z_1 Z_2 e^2}{\hbar \cdot v}$ is the Coulomb parameter, as well as the blurring of the interaction (diffuseness) $\Delta R = \frac{2.2\cdot(2l_1+1)\cdot\lambda_1}{k\cdot\left(\eta+\sqrt{\eta^2+l_1(l_1+1)}\right)}$.

Figure 9 shows the results of fitting data on the scattering of α-particles on ^{10}B nuclei in the energy range from 22.5 to 91.8 MeV using PPA.

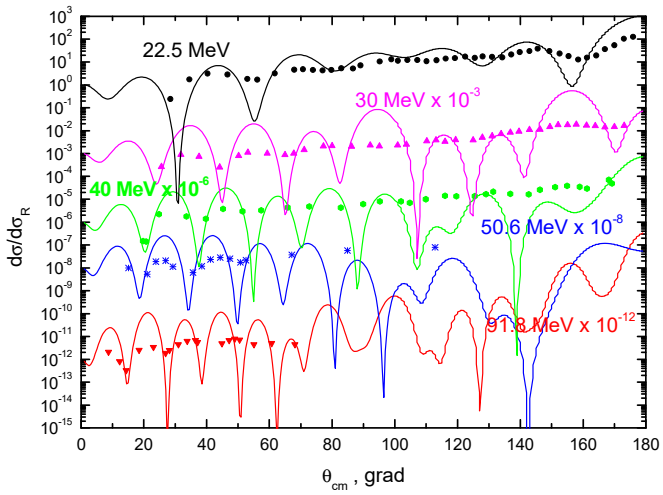

Figure 9. Angular distributions of differential cross sections of elastically scattered alpha-particles at ^{10}B with energies from 22.5 to 91.8 MeV. Points-experimental data taken from works [29–31]; curves-calculations within the framework of PPA.

The dependence of the free parameters of the PPA scattering matrix, the calculated interaction radii, and the blurring of the interaction in the elastic scattering of alpha-particles by ^{10}B are shown in Figures 10 and 11.

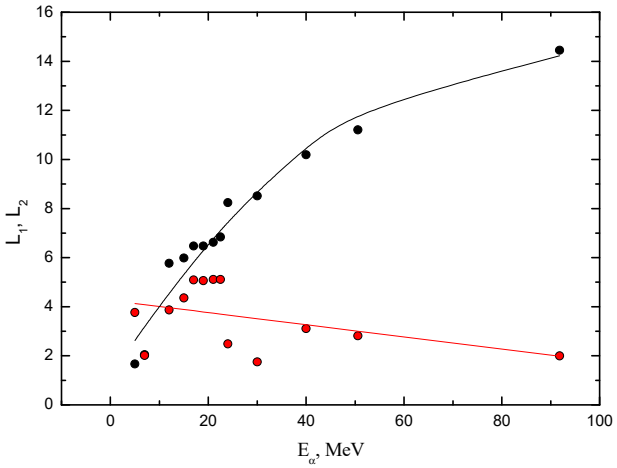

Figure 10. Dependence of the free parameters l_1 (black points) and l_2 (red points) of the PPA on the energy of incident alpha-particles. Dots—calculated values; curves—approximation of the obtained data.

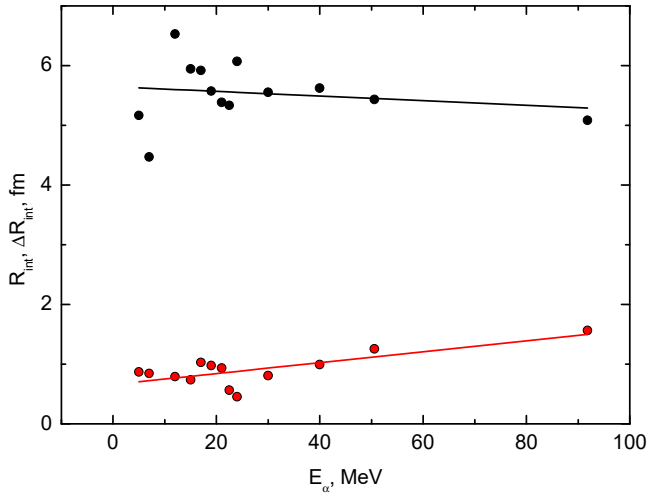

Figure 11. Dependence of the calculated interaction radius (black dots) and interaction blur (red dots) of the PPA on the energy of incident alpha-particles. Dots—calculated values; curves—approximation of the obtained data.

The results of the calculations of the free parameters of the scattering matrix and the geometric parameters of the studied reaction using the PPA are summarized in Table 2.

The core radius (R), according to [49], was determined as

$$R = R_{\text{int}} - R_{\alpha} - r_{NN},$$

where R_{α} is the alpha-particle radius, and r_{NN} = 1 fm is the range of nuclear forces. The calculated R values are summarized in Table 3 and shown in Figure 12.

It can be seen that at low energies, significant deviations of the calculated values of R from the classical radius are observed. This can most likely be explained by the uncertainty of scattering due to the long de Broglie wavelength of the incident particle. In addition, both resonance phenomena and the compound nucleus can play a significant role in this area. The radii of the ^{10}B nucleus in the high-energy region (30 MeV and above) extracted

from the PFA analysis are consistent with their values found from the analysis using the optical model.

Table 2. Free parameters of the scattering matrix in the PPA and the calculated geometric parameters of the elastic scattering of alpha-particles by ^{10}B.

E_α, MeV	l_1	l_2	λ_1	λ_2	B	R_{int}, fm	ΔR_{int}, fm
5	1.662	3.762	0.23	0.146	0.476	5.164	0.868
7	2.041	2.014	0.23	0.146	0.476	4.468	0.842
12	5.768	3.87	0.219	0.866	0.941	6.526	0.79
15	5.986	4.357	0.224	0.909	0.722	5.941	0.735
17	6.468	5.086	0.329	0.661	0.45	5.919	1.027
19	6.473	5.062	0.329	0.948	0.722	5.574	0.976
21	6.619	5.111	0.329	0.956	0.702	5.381	0.934
22.5	6.838	5.11	0.204	0.964	0.592	5.332	0.562
24	8.243	2.487	0.167	1.409	1.966	6.068	0.452
30	8.514	1.754	0.331	0.249	0.775	5.55	0.807
40	10.189	3.105	0.463	0.241	0.24	5.62	0.992
50.6	11.203	2.817	0.655	0.17	0.286	5.431	1.257
91.8	14.446	1.991	1.083	0.39	0.581	5.083	1.563

Table 3. Calculated ^{10}B radii from the elastic scattering of α-particles.

Eα, MeV	**5**	**7**	**12**	**15**	**17**	**22.5**	**24**	**30**	**40**	**50.6**	**91.8**
R_{10B}, fm	2.264	1.568	3.626	3.041	3.019	2.432	3.168	2.65	2.72	2.531	2.183

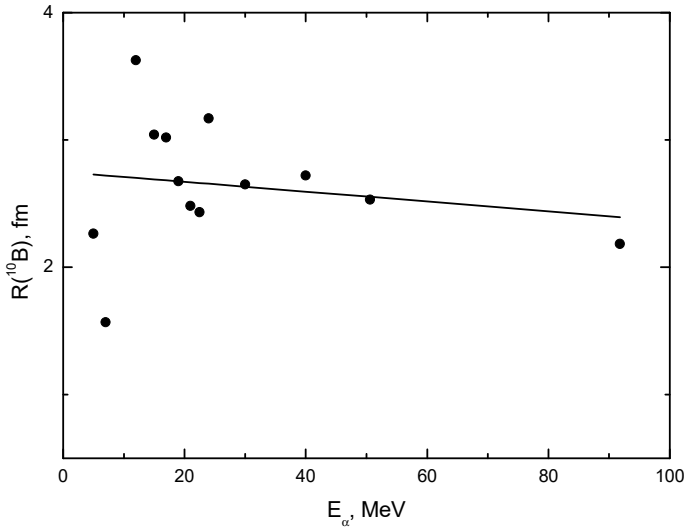

Figure 12. ^{10}B radii from elastic scattering of alpha-particles. Dots—calculated values; curve—classic radius.

3.3. Coupled-Channel Analysis

Since the ^{10}B nucleus is highly deformed [25,26], its low-lying states have a well-defined collective nature. In this case, the coupled-channel method is most suitable for describing scattering. Calculations were carried out using the FRESCO program [38] with the optical potential obtained from the analysis of elastic scattering with an optical model

with a set of parameters for an energy of 29 MeV (see Table 1). The calculation results for the elastic and inelastic scattering (transitions to the ground (3^+) and excited 0.718 (1^+) states of the ^{10}B nucleus) are compared with the experimental data in Figures 13 and 14. As can be seen from Figure 13, the calculated elastic scattering cross sections with set A from Table 1 (green curve) exhibit a pronounced diffraction structure over the entire range of angles. In the measured cross sections at large angles, it completely disappears, and a noticeable rise is observed with increasing scattering angle. This effect can be explained by the contribution to the scattering of the exchange mechanism with the transfer of the heavy ^{6}Li cluster. Calculations of the cluster exchange cross section were carried out using the FRESCO program. The wave functions of distorted waves for the input and output channels were calculated with the OPs taken from Table 1.

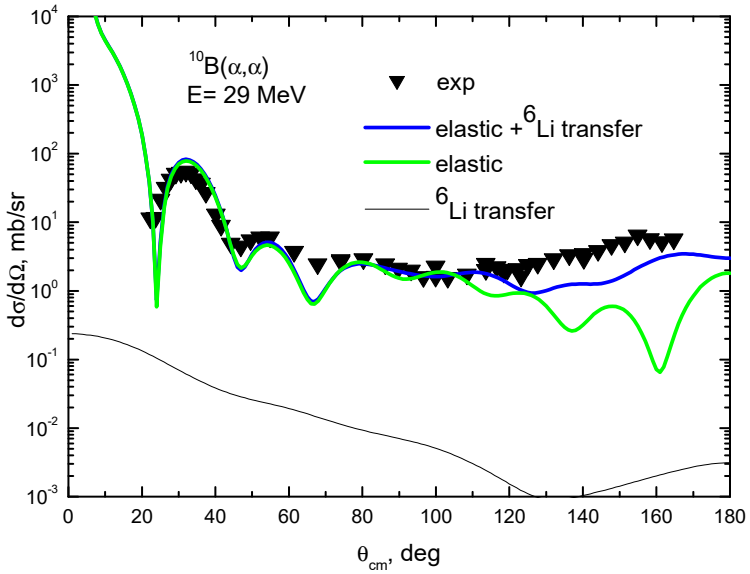

Figure 13. Angular distribution of CSs for elastic scattering with the transition to the ground state 3^+ of the ^{10}B nucleus. Symbols are experimental CSs. Green curv-calculation within the framework of the coupled-channel method using the FRESCO program. Black curve-calculation of the cross sections for the exchange process with the transfer of the ^{6}Li cluster in the ground state. Blue curve—calculation of elastic scattering taking into account the transfer of the ^{6}Li cluster.

The α+^{6}Li cluster wave function of the boron nucleus was calculated using the Woods–Saxon potential with a reduced radius of 1.25 fm and diffuseness of 0.65 fm. The depth of the potential was selected such that the required binding energy of the clusters was obtained.

The differential cross sections for the reaction ^{10}B(α,^{10}B)α were calculated using the following formula:

$$(d\sigma/d\Omega)_{\text{exp}} = S_1 S_2 \, (d\sigma/d\Omega)_{\text{th}}, \quad (11)$$

where $(d\sigma/d\Omega)_{\text{th}}$ is the calculated CSs, and S_1 and S_2 are the cluster spectroscopic factors of the ^{10}B in the input and output channels, respectively, in the α + ^{6}Li representation. The latter values are phenomenological parameters and are determined from a comparison of calculated cross sections with experimental data at large angles. An accurate account of this mechanism is complicated, however, by the fact that, in comparison with the transfer of light clusters d, t, ^{3}He, and α, the transfer of a heavy cluster is possible not only in the ground state but also in excited states, for which the spectroscopic amplitudes are unknown or known with insufficient accuracy. Therefore, for a rough assessment of the effect, the transfer of ^{6}Li was taken into account only in its ground (1^+) state (Figure 13). The spectroscopic amplitude for the cluster (α + ^{6}Li$_{\text{g.s.}}$) $1D$ wave function for the ground (3^+) state of the ^{10}B nucleus was chosen from the best description of the experiment at large angles, where, as can be seen from Figure 11, the transfer cross section of the ^{6}Li

nucleus makes the largest contribution to scattering. At a spectroscopic amplitude of 1.4, the calculation satisfactorily reproduces the character of experimental cross sections at large angles.

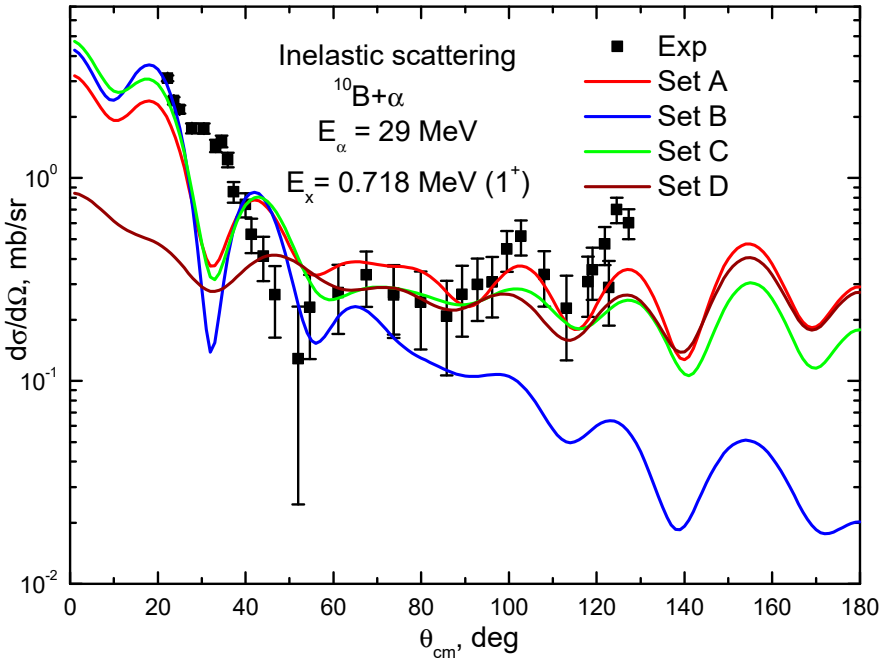

Figure 14. Angular distribution of inelastic scattering with the transition to the state E_x = 0.718 MeV (1^+) of the ^{10}B nucleus. Symbols are experimental CSs. Curves-calculations used in the coupled-channel method with the FRESCO program with optical potentials A, B, C, and D from Table 1, and the deformation parameter $\beta_2 = 0.60 \pm 0.15$.

This result is consistent with the results of the analysis of elastic scattering of ^{11}B(α, α)^{11}B at an energy of 50 MeV [50], where the rise in the cross section at reverse angles is explained by the exchange in the ^{7}Li cluster. At the same time, for excited states of the ^{11}B nucleus, the cluster transfer mechanism provides an increase in the cross section of only 30–50%. As indicated in [50], the existing differences are most likely the result of both an incomplete description of the transfer process, in which the possible contribution of other excited states of the ^{7}Li nucleus was not taken into account, and insufficient knowledge of the spectroscopic amplitudes.

In the angular distribution of the inelastic scattering with the transition to the excited state of the nucleus ^{10}B E_x = 0.718 MeV (1^+), shown in Figure 14, the diffraction structure is observed over the entire measured range of angles. In calculations that use the coupled-channel method [38,51,52], it was assumed that the interaction, following the deformation of the nuclear surface, is described by the optical potential $V(r, R(\theta'))$ with the radius parameter $R(\theta')$ depending on the polar angle θ' in a fixed coordinate system associated with the nucleus. In the case of axial symmetry, the parameter $R(\theta')$, considering only the quadrupole deformation, can be represented as

$$R(\theta') = R_0[1 + \beta_2 Y_{20}(\theta')], \quad (12)$$

where β_2 is the quadrupole deformation parameter.

Calculations were performed with all the sets from Table 1 (A, B, C, and D). As can be seen from Figure 14, calculations with sets A, C, and D provide an equivalent description of the angular distribution in the angular range 40°–120°. However, potential D produces underestimated cross sections at small angles, and potential B produces them at large angles. The deformation parameter β_2 was extracted from a comparison of calculated cross

sections with experimental data in the angular range 40°–120°. At $\beta_2 = 0.60 \pm 0.15$, the calculations are in good agreement with the experiment.

As can be seen from Figure 13, the analysis of elastic scattering, performed using the coupled-channel method, taking into account the possible contribution of the exchange mechanism with the transfer of the ^{6}Li cluster, provides a fairly good description of the experimental cross sections in the measured range of angles. The value of the quadrupole deformation $\beta_2 = 0.60$ for the ^{10}B nucleus obtained from the analysis of elastic and inelastic scattering of α-particles is consistent with the results of studies of the scattering of protons, deuterons, and ^{3}He [25,53–55].

4. Conclusions

At an energy of 29 MeV, the angular distributions of the cross sections for the elastic and inelastic scattering of α-particles on ^{10}B nuclei with excitation of the state $E_x = 0.718$ MeV (1^+) were measured. The analysis of the angular distributions measured by us, and the distributions measured earlier in the energy range of 24–90 MeV was carried out within the framework of the optical model and the coupled-channel method. Optimal parameters of optical potentials were found that make it possible to satisfactorily describe the experimental elastic scattering cross sections in a wide range of α-particle energies. Taking into account the contribution of the elastic transfer mechanism of the ^{6}Li cluster made it possible to reproduce correctly the rise of the cross section at the backward angles in the elastic channel. The remaining difference is most likely the result of both an incomplete description of the transfer process, in which the possible contribution of other excited states of the ^{6}Li nucleus was not taken into account, and insufficient knowledge of the spectroscopic amplitudes.

From the analysis of the inelastic scattering at an energy of 29 MeV on ^{10}B nuclei, the value of the quadrupole deformation parameter $\beta_2 = 0.60 \pm 0.15$ was extracted. Calculations based on parameterized phase analysis made it possible to determine the geometric parameters of the interaction potential. The radii of the ^{10}B nuclei in the high-energy region (30 MeV and above) obtained by PPA are in good agreement with the radii calculated in the framework of the optical model.

Author Contributions: Conceptualization, N.B.; data curation, M.N. (Maulen Nassurlla), R.K., D.A., D.Z., A.S. and D.I.; formal analysis, M.N. (Maulen Nassurlla); investigation, M.N. (Marzhan Nassurlla); methodology, S.S.; project administration, N.B.; resources, G.B., V.D., Y.M. and A.M. All authors have read and agreed to the published version of the manuscript.

Funding: This work was supported by the program #AP14870964 (Study of the processes of interaction of protons and ions ^{10}B with nuclei ^{11}B for thermonuclear and astrophysical applications) of the Ministry of Education and Science of the Republic of Kazakhstan.

Data Availability Statement: No new data were created or analyzed in this study. Date sharing is not applicable to this article.

Conflicts of Interest: The authors declare that they have no known competing financial interests or personal relationships that could have appeared to influence the work reported in this paper.

Abbreviations

The following abbreviations are used in this manuscript:

OP	Optical potential
OM	Optical model
PPA	Parameterized phase analysis
AD	Angular distribution
CSs	Cross sections

References

1. McFadden, L.; Satchler, J.R. Optical model analysis of the scattering of 24.7 MeV alpha particles. *Nucl. Phys. A* **1966**, *84*, 177. [CrossRef]
2. Igo, G.; Thaler, R.M. Optical model analysis of the elastic scattering of alpha particles. *Phys. Rev. C* **1957**, *106*, 126. [CrossRef]
3. Hodgson, P.E. The nuclear optical model. *Rep. Prog. Phys.* **1971**, *34*, 765. [CrossRef]
4. Goldberg, D.A.; Smith, S.M.; Burdzik, G.F. Refractive behavior in intermediate-energy alpha scattering. *Phys. Rev. C* **1974**, *10*, 1362. [CrossRef]
5. Khoa, D.T. α-nucleus optical potential in the double-folding model. *Phys. Rev. C* **2001**, *63*, 034007. [CrossRef]
6. Satchler, G.R.; Love, W.G. Folding model potentials from realistic interactions for heavy-ion scattering. *Phys. Rep.* **1979**, *55*, 183. [CrossRef]
7. Avrigeanu, M.; Avrigeanu, V. α-particle nuclear surface absorption below the Coulomb barrier in heavy nuclei. *Phys. Rev. C* **2010**, *82*, 014606. [CrossRef]
8. Bryant, H.C.; Jarmie, N. Nuclear glory scattering. *Ann. Phys.* **1968**, *47*, 127. [CrossRef]
9. Budzanowski, A.; Dudek, A.; Dymarz, R.; Grotowski, K.; Jarczyk, L.; Niewodniczański, H.; StrzaKowski, A. Glory effect in the optical-model analysis. In Proceedings of the International Conference on Nuclear Physics, Gatlinburg, Tennessee, 12–17 September 1966; Academic Press: New York, NY, USA, 1967.
10. Budzanowski, A.; Grotowski, K.; Strzalkowski, A. Back Scattering of Alpha Particles. *Acta Phys. Polon. A* **1970**, *38*, 631.
11. Bertero, B.; Carrassi, M.; Passatore, G.; Viano, G.A. Further Analysis of α-C^{12} Scattering Process by Regge Representation. *Nuovo Cim.* **1965**, *36*, 954. [CrossRef]
12. Gruhn, C.R.; Wall, N.S. Large-Angle Elastic Scattering of Alpha Particles by ^{39}K, ^{40}Ca, ^{42}Ca, ^{44}Ca and ^{50}Ti. *Nucl. Phys.* **1966**, *81*, 161. [CrossRef]
13. Ceuleneer, R.; Michel, F. Regge Poles and Backward Elastic α-Particle Scattering from ^{16}O. *Phys. Lett. B* **1973**, *43*, 365–367. [CrossRef]
14. Budzanowski, A.; Jarczyk, L.; Kamys, B.; Kapuscik, A. Mechanism of α-Particle Scattering from ^{28}Si Nuclei. *Nucl. Phys. A* **1976**, *265*, 461. [CrossRef]
15. Cowley, A.A.; Heymann, G. Regge Pole Analysis of the Elastic Scattering of α-Particles from ^{16}O. *Nucl. Phys. A* **1970**, *146*, 465. [CrossRef]
16. McVoy, K.W. Regge Poles and Strong Absorption in Heavy-Ion and α-Nucleus Scattering. *Phys. Rev. C* **1971**, *3*, 110. [CrossRef]
17. Frahn, W.E. Angular-momentum matching in the strong-absorption model. *Lett. Nuovo Cim.* **1971**, *1*, 561–564. [CrossRef]
18. von Oertzen, W. On the interaction induced by the exchange of nucleons between two identical nuclear cores. *Nucl. Phys. A* **1970**, *148*, 529. [CrossRef]
19. Gridnev, K.A.; Ogloblin, A.A. Anomalous Backward Scattering and Quasi-molecular Structure of Nuclei. *Fiz. Elem. Chastits At. Yadra.* **1975**, *6*, 393, *Sov. J. Particles Nucl.***1976**, *6*, 158.
20. Freer, M. The clustered nucleus–cluster structure in stable and unstable nuclei. *Rep. Prog. Phys.* **2007**, *70*, 2149. [CrossRef]
21. Beck, C. (Ed.) *Clusters in Nuclei*; Lecture Notes in Physics; Springer Science & Business Media: New York, NY, USA, 2010; Volume 1, p. 818.
22. Pakou, A.; Sqouros, O.; Soukeros, V.; Cappuzzello, F. Global description and decay rates for continuum excitation of weakly bound nuclei. *Eur. Phys. J. A* **2021**, *57*, 25. [CrossRef]
23. Shapiro, I.S. Dispersion theory of direct nuclear reactions. In *Selected Topics in Nuclear Theory*; Lectures Given at IAEA, Vienna; International Atomic Energy Agency (IAEA): Vienna, Austria, 1963.
24. Noble, J.V.; Coelho, H.T. Cluster-Model Vertex Functions for ^{16}O: Backward α-Particle Scattering. *Phys. Rev. C* **1970**, *1*, 385. [CrossRef]
25. Tilley, D.R.; Kelley, J.H.; Godwin, J.L.; Millener, D.J.; Purcell, J.; Sheu, C.G.; Weller, H.R. Energy Levels of Light Nuclei A = 10. *Nucl. Phys. A* **2004**, *745*, 155. [CrossRef]
26. Bohr, A.; Mottelson, B.R. *Nuclear Structure. Volume II Nuclear Deformations*; World Scientific Publishing Co. Pte. Ltd.: New York, NY, USA; Amsterdam, The Netherlands, 1998.
27. Burtebayev, N.; Sakuta, S.B.; Nassurla, M.; Saduev, N.; Nassurlla, M.; Sadykov, T.K.; Trzcińska, A.; Wolińska-Cichocka, M.; Khojayev, R. Mechanism of the ^{11}B(α, *t*)^{12}C reaction at an energy of 40 MeV, role of exchange processes and collective Excitations. *Eur. Phys. J. A* **2019**, *55*, 38. [CrossRef]
28. Nassurlla, M.; Burtebayev, N.; Sakuta, S.B.; Karakozov, B.K.; Nassurlla, M.; Burtebayeva, J.; Khojayev, R.; Sabidolda, A.; Yergaliuly, G. Deuteron scattering and (*d*, *t*) reaction on ^{11}B at an energy of 14.5 MeV. *Nucl. Phys. A* **2022**, *1023*, 122448. [CrossRef]
29. David, P.; Debrus, J.; Mommsen, H.; Riccato, A. Elastic scattering of α-particles on ^{10}B for E_α = 5-30 MeV. *Nucl. Phys. A* **1972**, *182*, 234. [CrossRef]
30. Bentheim, F.; David, P.; Debrus, J.; Hinterberger, F.; Jahn, R.; Lubke, F.; Mommsen, H.; Schoenmachers, R.; Schuller, B. Elastic scattering of α-particles on ^{10}B for E_α = 5−50 MeV. *Z. Phys. A* **1976**, *279*, 163. [CrossRef]
31. Jarczyk, L.; Kamys, B.; Rudy, Z.; Strzalkowski, A.; Styczen, B.; Berg, G.P.A.; Magiera, A.; Meissburger, J.; Oelert, W.; Rossen, P.; et al. Triton and helion transfer in the ^{10}B(α,^{7}Li)^{7}Be reaction at E_{lab}= 91.8 MeV. *Z. Physic A At. Nucl.* **1985**, *322*, 221. [CrossRef]
32. Hagino, K.; Ogata, K.; Moro, A.M. Coupled-channels calculations for nuclear reactions: From exotic nuclei to superheavy elements. *Prog. Part. Nucl. Phys.* **2022**, *125*, 103951. [CrossRef]

33. Perey, F. (The Niels Bohr Institute, Copenhagen, Denmark) SPI-GENOA an optical model search code. 1976; (Unpublished work).
34. Nilsson, B.S. SPI-GENOA an optical model search code. In *Niels Bohr Institute Computer Program Library*; Niels Bohr Institute: Copenhagen, Denmark, 1975.
35. Cheston, W.B.; Glassgold, A.E. Elastic scattering of alpha particles with optical model. *Phys. Rev. C* **1957**, *106*, 1215. [CrossRef]
36. Kucuk, Y.; Guimaraes, V.; Carlson, B.V. Towards a systematic optical model potential for A=8 projectiles. *Eur. Phys. J. A* **2021**, *57*, 87. [CrossRef]
37. Baktybaev, M.K.; Basybekov, K.B.; Burtebaev, N.; Artemov, S.V.; Blechman, A.M.; Dyusebaev, B.A.; Duysebaev, A.; Gulamov, I.R.; Ismailov, K.M.; Zhurynbaeva, G.S.; et al. The (a,t) and (a,^{3}He) cross section data at the energies 40.0 and 50.5 MeV. I. In Proceedings of the Eurasia Conference on Nuclear Science and Its Application, Izmir, Turkey, 23–27 October 2000; pp. 534–535.
38. Thompson, I.J. Coupled reaction channels calculations in nuclear physics. *Comput. Phys. Rep.* **1988**, *7*, 167. [CrossRef]
39. Nolte, M.; Machner, H.; Bojowald, J. Global optical potential for α particles with energies above 80 MeV. *Phys. Rev. C* **1987**, *36*, 1312. [CrossRef] [PubMed]
40. Farid, M.E.A.; Mahmoud, Z.M.M.; Hassan, G.S. Analysis of heavy ions elastic scattering using the double folding cluster model. *Nucl. Phys. A* **2001**, *691*, 671. [CrossRef]
41. Khoa, D.T.; Von Oertzen, W.; Bohlen, H.G. Double-folding model for heavy-ion optical potential: Revised and applied to study C12 and O16 elastic scattering. *Phys. Rev. C* **1994**, *49*, 1652. [CrossRef] [PubMed]
42. Cook, J. DFPOT-A program for the calculation of double folded potentials. *Comput. Phys. Commun.* **1982**, *25*, 125. [CrossRef]
43. Aygun, M.A. Comprehensive analysis of elastic scattering of ^{14}N projectile on ^{7}Li, ^{9}Be, ^{11}B, ^{12}C, ^{16}O, ^{26}Mg, ^{28}Si, ^{40}Ca, ^{56}Fe, ^{59}Co, ^{60,62}Ni, ^{70,74}Ge, ^{90}Zr, ^{112}Cd, ^{118}Sn, ^{159}Tb and ^{197}Au at various incident energies. *Chin. J. Phys.* **2017**, *55*, 2559. [CrossRef]
44. De Vries, H.; De Jager, C.W.; De Vries, C. Nuclear charge-density-distribution parameters from elastic electron scattering. *At. Data Nucl. Data Tables* **1987**, *36*, 495. [CrossRef]
45. Akhiezer, A.I.; Pomeranchuk, I.A. Diffraction Phenomena in Collisions of Fast Particles with Nuclei. *UFN* **1958**, *65*, 593. [CrossRef]
46. Akhiezer, A.I.; Berezhnoy, Y.A.; Pilipenko, V.V. Quantum Interferention and Nuclear Optics. *Phys. El. Part. At. Nucl.* **2000**, *31*, 457.
47. Berezhnoy, Y.A.; Molev, A.S. Interference between diffractive, refractive and Coulomb effects in the cross section for the elastic scattering of light nuclei by nuclei at intermediate energies. *Phys. At. Nucl.* **2004**, *67*, 1454. [CrossRef]
48. Gonchar, V.Y. Investigation of uniqueness of parameters in the method of phase shifts. *Phys. At. Nucl.* **1969**, *9*, 987.
49. Yushkov, A.V. Surface of $b(Z, N)$ Deformation for Nuclei with Z from 2 to 102. *Phys. El. Part. At. Nucl.* **1993**, *24*, 348.
50. Burtebayev, N.; Baktybayev, M.K.; Duisebayev, B.A.; Sakuta, S.B.; Peterson, R.D. Scattering of 40- and 50- MeV α particles from ^{11}B nuclei. *Phys. At. Nucl.* **2005**, *68*, 1356–1367.
51. Spatafora, A.; Cappuzzello, F.; Carbone, D.; Cavallaro, M.; Lay, J.A.; Acosta, L.; Numen Collaboration. ^{20}Ne + ^{76}Ge elastic and inelastic scattering at 306 MeV. *Phys. Rev. C* **2019**, *100*, 034620. [CrossRef]
52. Carbone, D.; Linares, R.; Amador-Valenzuela, P.; Calabrese, S.; Cappuzzello, F.; Cavallaro, M.; Firat, S.; Fisichella, M.; Spatafora, A.; Acosta, L.; et al. Initial State Interaction for the ^{20}Ne + ^{130}Te and ^{18}O + ^{116}Sn Systems at 15.3 AMeV from Elastic and Inelastic Scattering Measurements. *Universe* **2021**, *7*, 58. [CrossRef]
53. Ajenberg-Selove, F. Energy levels of light nuclei A = 5–10. *Nucl. Phys. A* **1988**, *490*, 1–225. [CrossRef]
54. Swiniarski, R.; Resmini, F.G.; Glashausser, C.; Bacher, A.D. Study of ^{10}B by inelastic Scattering of 30.3 MeV protons. *Helv. Phys. Acta* **1976**, *49*, 227.
55. Squier, G.T.A.; McClatchie, E.A.; Johnston, A.R.; Batten, R.J.; England JB, A.; Kingston, F.G. Elastic and Inelastic Scattering of ^{3}He Particles from ^{10}B at 32 MeV. *Nucl. Phys. A* **1968**, *119*, 369. [CrossRef]

Disclaimer/Publisher's Note: The statements, opinions and data contained in all publications are solely those of the individual author(s) and contributor(s) and not of MDPI and/or the editor(s). MDPI and/or the editor(s) disclaim responsibility for any injury to people or property resulting from any ideas, methods, instructions or products referred to in the content.